Observation of femtosecond infrared luminescence in gold

Tohru Suemoto,[1,*] Ken-ichi Yamanaka,[2] and Noriaki Sugimoto[2]
[1]*Toyota Physical and Chemical Research Institute, Yokomichi 41-1, Nagakute Aichi, 480–1192, Japan*
[2]*Toyota Central R&D Labs., Inc.. Yokomichi 41-1, Nagakute Aichi, 480–1192, Japan*

(Received 25 April 2019; revised manuscript received 10 July 2019; published 5 September 2019)

Femtosecond infrared luminescence in Au was observed using the upconversion technique. The instantaneous luminescence intensity for a sample with an appropriate surface roughness was three orders of magnitudes higher than that for a flat film and comparable to the hot luminescence in InAs. The time-resolved spectra from 0 to 1 ps exhibited broad features spreading from 0.3 to 1.04 eV, indicating a continuous joint density of states around the Fermi energy. In terms of a simple model that considers nonthermal and thermal carriers for describing the hot luminescence, most of the characteristic behaviors are semiquantitatively understood.

DOI: 10.1103/PhysRevB.100.125405

I. INTRODUCTION

Luminescence is a standard tool for investigating the excited electronic states and their relaxation dynamics in semiconductors [1–3] and insulators, which have an energy gap to prohibit the fast nonradiative carrier recombination process. In gapless materials such as metals and semimetals, the photoexcited carriers relax very quickly, mainly owing to the electron-phonon interaction, before emitting an appreciable amount of luminescence photons. However, luminescence from graphite [4], which is known as a semimetal, and that from metallic surface states of a topological insulator [5], was recently observed using femtosecond time-resolved luminescence spectroscopy. The instantaneous intensity of the luminescence in these materials is relatively high, allowing us to investigate the excited state dynamics using femtosecond luminescence spectroscopy.

Regarding the luminescence from elemental metals, little information has been collected in the half century since the discovery of luminescence in noble metals. Visible luminescence from Au and Cu—under irradiation with a blue laser (wavelength of 488 nm)—was reported by Mooradian [6] in 1969. The luminescence was attributed to *interband* radiative recombination between electrons near the Fermi level and the holes created in the first *d* band, which is far below the Fermi energy.

The discovery of surface-enhanced Raman scattering [7], which appears on noble metals with roughened surfaces, led to a renewed interest in the luminescence from metals in the 1980s. A comprehensive investigation of the luminescence in carefully controlled surfaces of Au, Ag, and Cu in ultrahigh vacuum was performed by Boyd *et al.* [8]. Based on the excitation energy dependence of the spectra, the mechanism of recombination luminescence involving *d* band holes was established. The quantum yield was estimated to be on the order of 10^{-10} for the smooth surfaces, and the intensity was one or two orders of magnitude higher for rough surfaces. This enhancement has been ascribed to the localized surface plasmon resonance, as in the case of surface enhanced Raman scattering [7].

However, concerning the dynamical behavior of luminescence in metals, very little information is available. Although the time response of luminescence from a rough Au film was reported, only the upper limit of the lifetime was presented (2.3 ps) [9].

In this paper, we present the time-resolved infrared (IR) luminescence from Au, which is a demonstration of the femtosecond luminescence in metals. With roughened surfaces, the instantaneous intensity was enhanced three orders of magnitude and comparable to that observed in InAs, which is known as a direct-gap semiconductor. A simple model considering the nonthermal and thermalized electrons is introduced to interpret the basic behavior of the luminescence, and the IR luminescence in Au is ascribed to the *intraband* radiative transitions across the Fermi surface. Additionally, the three orders of magnitude enhancement of the luminescence intensity by roughening the surface was ascribed to the increases in the absorbance and emissivity.

II. EXPERIMENT

We employed the upconversion technique [10] to perform luminescence measurements with femtosecond time resolution. Mode-locked pulses at a wavelength of 1036 nm (1.19 eV) and a repetition rate of 100 MHz from a Yb-fiber laser were amplified with a Yb-fiber amplifier to an average power of 600 mW (fluctuation stabilized below 1%) and divided into pumping and gating pulses. The pumping beam was focused on the sample with a spot diameter of 20 μm. The luminescence pulses from the sample were collected and focused on a nonlinear optical crystal (lithium iodate, LIO) by using two paraboloidal mirrors and frequency mixed with the gating pulses. The laser light and the second harmonic from the LIO crystal were blocked by a shortwave-pass filter and a longwave pass filter, respectively. The anti-Stokes luminescence, which may overlap in wavelength with the sum frequency, was removed by passing the luminescence through

*suemoto@toyotariken.jp

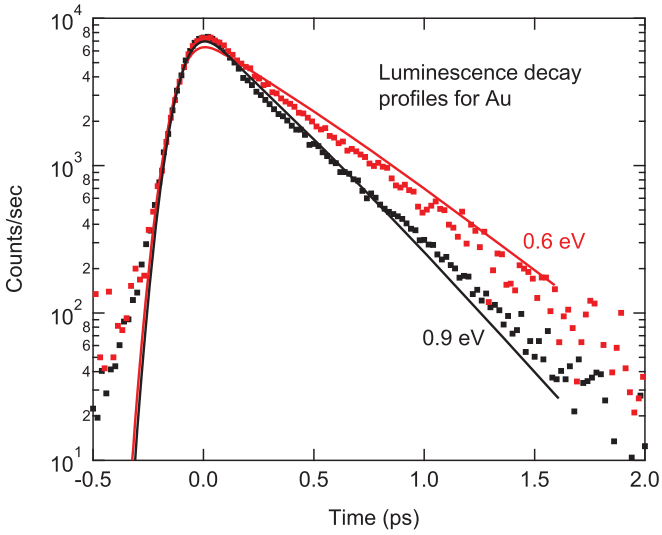

FIG. 1. Normalized luminescence decay profiles at 0.9 (black) and 0.6 eV in Au (red) with an excitation power of 145 mW. Experimental and calculated results are shown by squares and solid curves, respectively.

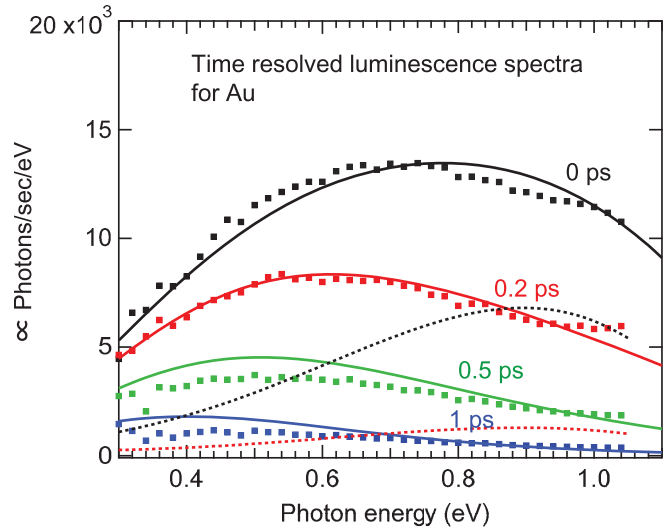

FIG. 2. Time-resolved luminescence spectra for Au at 0 ps (black), 0.2 ps (red), 0.5 ps (green), and 1 ps (blue). The experimental and calculated results are shown by squares and solid curves, respectively. The dotted curves are nonthermal components at 0 ps (black) and 0.2 ps (red) calculated in the model.

a Si filter placed between two paraboloidal mirrors. The time shift due to group velocity dispersion in Si was compensated numerically in the data acquisition.

The generated sum frequency light was directed to a band-pass filter (Semrock TBP01 series), which was exchangeable and tuned by changing the incident angle, and detected by a cooled photomultiplier (Hamamatsu R943-02). This system had a sensitivity between 1.05 and 0.3 eV and a time resolution of 200 fs (full width at half maximum). The sensitivity of the system, including the upconversion efficiency, was calibrated by observing the upconverted signal of a W-lamp with a sapphire window (HELIOWORKS EP-3965; color temperature 1900 K) between 0.3 and 1.07 eV. The time-resolved spectra were plotted on a scale proportional to the photon numbers per unit energy window per unit time. All measurements were performed in air at room temperature.

The metal samples that we used were commercially available Au plates. The surfaces were roughened with sand-blasting, grinding paper or diamond paste. The samples were excited at $E_{\mathrm{exc}} = 1.19$ eV and continuously rotated in a plane to avoid degradation due to prolonged laser irradiation and to average the effect of surface roughness. For the measurements shown in Figs. 1–3, we use a sample roughened by sand-blast technique with 6-μm particles. The surface profiles are probed by a laser confocal microscope (Keyence VK-9700). For the measurement of absorption, we used a calorimeter, which measures the temperature increase of a sample piece with a thermistor under irradiation of 100-mW laser light.

III. RESULTS

The decay profiles of the luminescence at $E_{\mathrm{L}} = 0.9$ and 0.6 eV are shown in Fig. 1. As the curves exhibit an asymmetric shape around the peak, the signal is not ascribed to the sum frequency of Rayleigh scattering, which should reflect the laser pulse shape directly. The possibility of white-light generation via a nonlinear process, such as self-phase modulation, is also rejected, because the intensity is not far from linear (exponent of 1.3–1.47) dependence on the pumping power, as mentioned later. Because the Au surface is inert in air, we do not expect any contributions from oxides or other compounds on the surface. Therefore, the signal is ascribed to the intrinsic luminescence of Au. The decay curves are slightly nonexponential and that for 0.6 eV shows longer lifetime than 0.9 eV.

Figure 2 shows the time-resolved luminescence spectra. All the curves are plotted on a scale proportional to the photons/s per unit energy window. The spectral shape slightly depends on the roughness of the surface, which could not be fully controlled. Nevertheless, we observe important common features in the spectra. First, they spread over the whole measurement range without any pronounced structures. The broad feature suggests the continuous density of states (DOS) for the electrons and holes involved in the radiative transition, as expected in metals. As the decrease is faster at a high photon energy (e.g., at 1 eV) than at a lower photon energy (e.g., 0.6 eV), the spectrum weight moves to a lower energy over time, indicating cooling and/or thermalization processes of the electrons at the subpicosecond timescale.

The excitation-power dependences of the decay profiles measured at 0.9 eV are shown in Fig. 3(a). Here, 100% power corresponds to an excitation power of 145 mW applied to irradiate a 20-μm-diameter spot on the sample surface. We observe that the lifetime decreases as the excitation power decreases from 100% to 20%. The luminescence intensity at 0.9 eV evaluated at the peak is shown in Fig. 3(b), where we observe a superlinear power dependence.

IV. DISCUSSION

To identify the origin of the luminescence in Au, we refer to the band structure near the X point illustrated in Fig. 4(a).

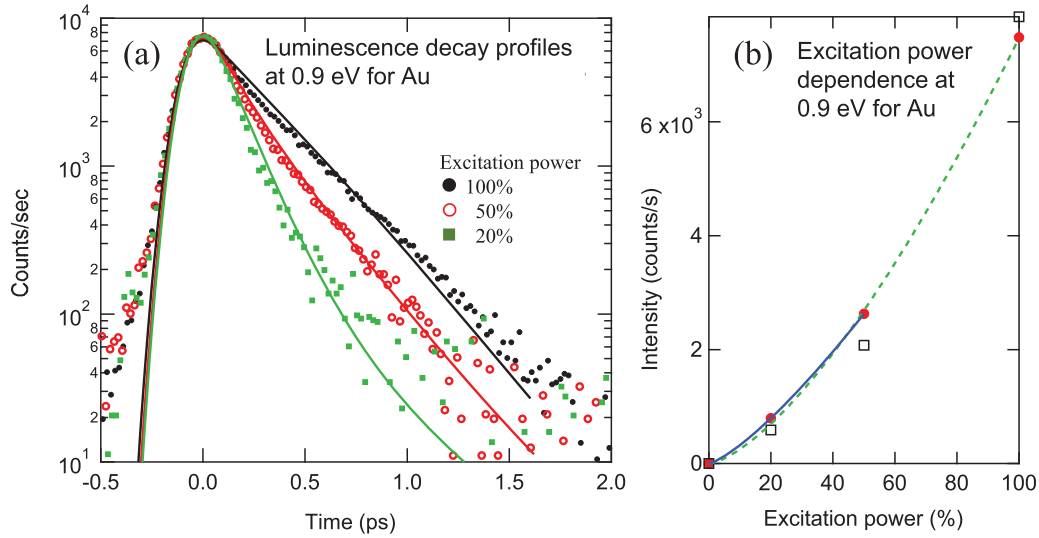

FIG. 3. (a) Excitation power dependence of the decay profiles at 0.9 eV in Au. The pump powers are 100% (black solid circles), 50% (red open circles), and 20% (green squares) of the full power (145 mW). The solid curves represent the calculated results for each excitation power (shown with corresponding color). (b) The power dependence of the luminescence intensity evaluated at the peak position at 0. 9 eV (red circles). The solid and dashed curves are the fitting to the data points up to 50% and 100%, showing $I^{1.3}$ and $I^{1.47}$ dependences, respectively. The calculated results are shown by open squares.

Here, the top of the *d* band, which is responsible for the well-known visible optical transitions, is located 2.1 eV below the Fermi level. Although the interband (vertical) transition between the *sp* band and the *d* band is also possible near the L point and K point, the energy separation is >2 eV. Therefore, the IR laser (1.19 eV) used in our experiment cannot induce any interband absorption or emission. Two-photon absorption can contribute to the luminescence at a very high excitation intensity, but it is unlikely to be the main process, because the excitation-power dependence at low excitation power (<50%), is close to linear (exponent of 1.3), as shown in Fig. 3(b). This is supported by the results of a previous time-resolved photoemission spectroscopy (TrPES) study performed under similar excitation conditions, in which the experimental observation was explained by a one-photon process [11].

The IR luminescence spectrum (time-integrated) for a rough Au surface was reported by Beverslius *et al.* [9]. Using 780-nm (1.58 eV, 120 fs) excitation, they found that the excitation-power dependence of the luminescence between 850 and 1000 nm was linear, in contrast to the quadratic dependence of the visible luminescence associated with the

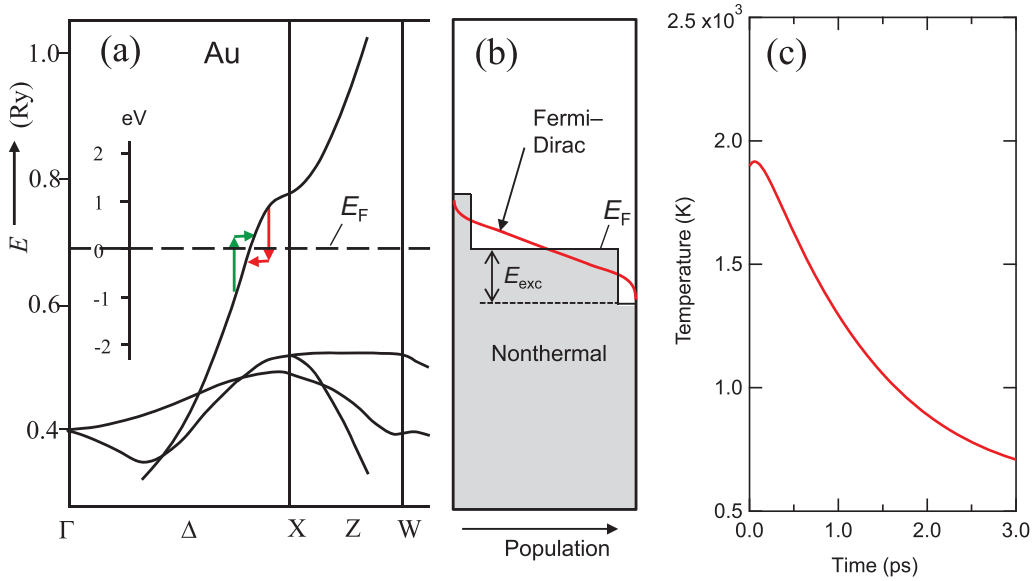

FIG. 4. (a) Band structure of Au near X point reconstructed from Ref. [12]. The arrows indicate intraband transitions corresponding to absorption (green) and emission (red). (b) Thermal (red curve) and nonthermal (grey hatched) distributions of electrons. (c) Time development of the electron temperature calculated in the model.

interband transition involving the d band. Thus they attributed the IR luminescence to one-photon excited intraband transitions within the conduction band, while the visible luminescence was ascribed to two-photon excitation from the d band to the states above the Fermi surface. Similarly, in our case, the absorption of the IR photons is assigned to one-photon intraband transitions near the Fermi level. Although the wavelength range studied is longer than theirs (>1200 nm), we expect that the same principle applies. The momentum-conservation rule in the intraband transition may be fulfilled by electron-electron scattering, electron-phonon interaction, or the surface roughness.

Regarding the electronic-relaxation dynamics in metals, numerous theoretical studies [13–16] have been performed since the 1990s, motivated by progress [17,18] in experiments using pump-probe techniques. However, in these theories, the luminescence was not explicitly treated. Therefore, we construct a very simple model to elucidate the basic behaviors of metal luminescence.

A. The model for metal luminescence

The luminescence intensity at a photon energy E_{L} is given by

$$\mathrm{L}(E_{\mathrm{L}}) = \varepsilon(E_{\mathrm{exc}})\varepsilon(E_{\mathrm{L}})WE_{\mathrm{L}}^3 \times \int_{-\infty}^{\infty} f\,(x)\,(\,1 - f(x - E_{\mathrm{L}}))D(x)D(x - E_{\mathrm{L}})dx, \tag{1}$$

where $\varepsilon(E_{\mathrm{L}})$ is the emissivity at E_{L}; $\varepsilon(E_{\mathrm{exc}})$ is the absorption at E_{exc}, which is equivalent to the emissivity according to Kirchhoff's law of thermal radiation; and W is the radiative recombination probability. Because the dispersion of the conduction band in Au near the Fermi surface is nearly straight, the DOS $D(x)$ at energy x can be assumed to be constant near E_{F}. The time-dependent distribution function of the nonequilibrium electron cannot be treated easily and is still under intense debate, because the system is in a highly nonequilibrium state and the thermalization and cooling processes proceed simultaneously. Therefore, for simplification, the nonthermal and thermal components are often separated [11,19]. The electron-decay dynamics in Au were studied by Fann *et al.* [11] using TrPES. The existence of a nonthermal distribution at the early stage was indicated by the energy spectrum of photoemission, which had a long high-energy tail extending to the excitation photon energy (1.84 eV), far above the thermal distribution. They successfully interpreted the time-resolved spectra according to the sum of the thermal and nonthermal distributions. Here, we adopt this formulation. The electron-distribution function is expressed as

$$f(x) = f_{FD}(x) + f_{\mathrm{NT}}(x). \tag{2}$$

The Fermi-Dirac distribution is given by

$$f_{FD}(x) = \frac{1}{e^{x/kT} + 1}. \tag{3}$$

Although the chemical potential at a finite temperature should generally be determined to keep the number of electrons constant, it can be set as E_{F} while the DOS is assumed to be constant near E_{F}.

The nonthermal distribution is expressed by a stepwise function [13]:

$$f_{\mathrm{NT}}(x) = \begin{cases} n_{NT}[1 - \theta(x - E_{\mathrm{exc}})], & \text{for } x > 0 \\ 1 - n_{NT}[1 - \theta(-x - E_{\mathrm{exc}})], & \text{for } x < 0, \end{cases} \tag{4}$$

where $\theta(x)$ is the unit step function, and n_{NT} is the population of nonthermal electrons, which are assumed to be produced instantaneously at the excitation.

For the thermal electron system, we assume preheating temperature T_{p} at $t = 0$. Since the excitation pulse has a finite time width, the system will have some thermalized electron at $t = 0$, due to the first half of the excitation pulse. In addition, a very fast e-e scattering process will produce low energy electrons, which are recognized as thermal electrons. These effects could contribute to the preheating of the electron system.

For the population of nonthermal electrons, we assume an exponential decay given by

$$n_{NT}(t) = n_0 e^{-t/\tau_1}. \tag{5}$$

Here, the initial population of nonthermal electrons n_0 is proportional to the excitation power. The thermal electrons, which obey the Fermi-Dirac distribution, are further heated by receiving energy from nonthermal electrons, and the temperature increases, compensating for the decrease in the population of nonthermal electrons. Total energy of the preheated and nonthermal electrons should be equal to the light energy absorbed by the sample. Then, assuming that the specific heat of the electron system is proportional to the electron temperature, the electron temperature is given as

$$T(t) = \left[\left({T_p}^2 + \left({T_0}^2 - {T_p}^2\right)(1 - e^{-t/\tau_1})\right)e^{-t/\tau_2} + {T_{RT}}^2\right]^{1/2}, \tag{6}$$

where T_{RT} is the asymptote temperature at $t = \infty$; τ_1 and τ_2 are the time constants for thermalization and cooling, respectively; and T_0 is the nominal maximum temperature, i.e., the final temperature of the thermal electron system, when the cooling is neglected. As the energy-transfer efficiency is unknown, T_0 is treated as an adjustable parameter.

B. Interpretation of spectra, time evolution, and power dependence

By using the experimental condition $E_{\mathrm{exc}} = 1.19\,\mathrm{eV}$ and setting the free parameters as $\tau_1 = 0.12$ ps, $\tau_2 = 0.9$ ps, $T_0 = 2000\,\mathrm{K}$, $T_{\mathrm{p}} = 1800\,\mathrm{K}$, $T_{\mathrm{RT}} = 600\,\mathrm{K}$, and $n_0 = 0.005$, we attempt to reproduce the experimental results. Figure 4(c) shows the time evolution of the calculated temperature; the real maximum electron temperature in this calculation is 1915 K. This is not far from the value of 1680 K determined via TrPES under similar excitation conditions [11]. We can reproduce the decay profiles in Fig. 1 and the increasing tendency of the lifetime at a low energy. In this calculation, we convolute the instrumental function with a time resolution of 200 fs.

The calculated time-resolved spectra are indicated by solid curves in Fig. 2. The time development of the spectrum from 0 to 1 ps, particularly the movement of the spectrum weight

toward a lower energy during decay, is well reproduced. The dotted curves represent the contribution of nonthermal components at 0 and 0.2 ps in calculation. We can see that the fast decay of the intensity at high energy part is mainly ascribed to the decay of the nonthermal component. The lifetime of nonthermal distribution, 0.12 ps, assumed in our model is consistent with TrPES experiments, because persistence of the nonthermal distribution at 400 fs has been observed [11], and the lifetime of electrons at 1 eV above Fermi energy is reported as 70 fs [20].

The luminescence intensity at lower excitation power is calculated as follows:

As the number of the nonthermal electrons will be proportional to the input energy I, we assume,

$$n_0(\mathrm{I}) = \frac{I}{I_0}\, n_0(I_0), \tag{7}$$

where I_0 is the input energy at full power excitation.

As the preheating temperature and the nominal maximum temperature will be proportional to square root of the input energy

$$T_0(\mathrm{I}) = (I/I_0)^{1/2}\, T_0(I_0) \tag{8}$$

and

$$T_\mathrm{p}(\mathrm{I}) = (I/I_0)^{1/2}\, T_\mathrm{p}(I_0) \tag{9}$$

are assumed. The decreasing tendency of the lifetime at low excitation powers in Fig. 3(a) is also nicely reproduced in the calculation. The maximum temperatures for 100, 50, and 20% power in the model are 1915, 1411, and 1014 K, respectively. The decay profiles seen after 0.5 ps are recognized as the cooling process of the thermalized electrons, because the nonthermal component after 0.2 ps is negligible, as seen in Fig. 2. The faster decay at lower excitation power is a consequence of the faster decay of the high energy tail of thermal distribution, when the initial temperature is low.

In this model, the power dependence of the intensity at the peak is superlinear in agreement with the experimental results, as shown in Fig. 3(b). At higher excitation density, the exponent of the power law is larger than 1.3, because the excessive heating of the electrons make an increasing contribution at 0.9 eV. It is worth noting that we do not need to consider two photon absorption for understanding this superlinear power dependence.

In spite of the simplicity of the model, the agreement with the experiment is extremely good. According to these results, we conclude that the femtosecond luminescence that we observed is an intrinsic effect of Au and reflects the dynamics of photoexcited carriers of the bulk material. Thus, the femtosecond luminescence provides direct dynamic information for the nonequilibrium electron system in a wide energy range.

C. Effect of surface roughness

The spectrum of the emissivity $\varepsilon(E_\mathrm{L})$ may modify the luminescence spectrum observable outside the metal. The emissivity responsible for radiating the luminescence is expected to be the same as that for thermal radiation, because both types of radiation originate from the thermally distributed electrons (neglecting the contribution from IR-active phonons, which is absent in Au). The effect of the surface morphology on the emissivity for thermal radiation [21] from metals has been extensively studied in artificially fabricated regular structures of Pt [22], W [23], heavily doped Si [24], roughened brass [25], etc. It is generally known that the emissivity is enhanced by surface roughness with a characteristic lateral correlation length close to the relevant wavelength.

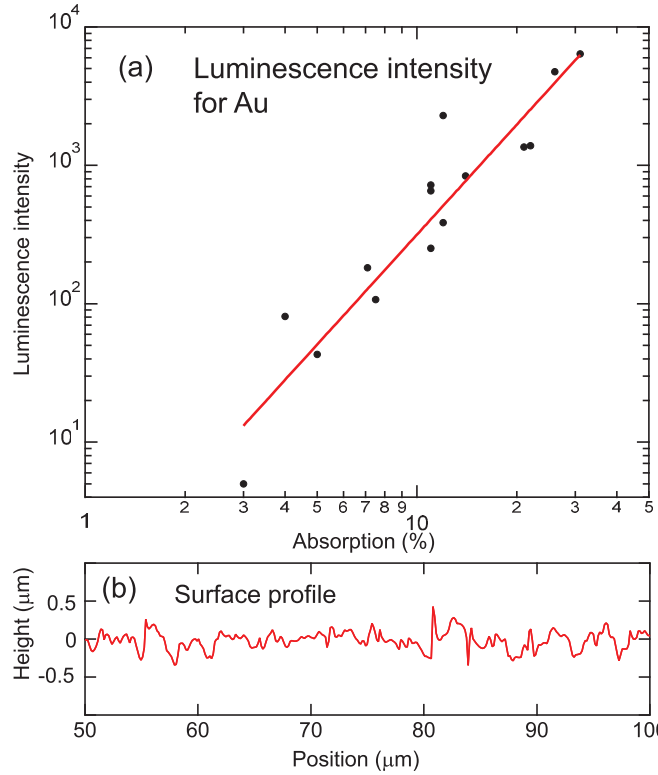

FIG. 5. (a) Luminescence intensity in Au with various surface roughness evaluated at 0.9 eV and $t = 0$ ps plotted as a function of absorption (%). The solid line is a fitting by power function $L \propto A^{2.64}$. (b) Typical surface profile measured by laser confocal microscope for sand-blasted sample.

To understand the three orders of magnitude enhancement of the luminescence intensity, we examined the correlation between the absorption strength and luminescence intensity. The absorption was evaluated at a wavelength of 1036 nm with a calorimeter, and the luminescence intensity was evaluated at the peak of the wave form at 0.9 eV. Figure 5(a) shows a plot of the luminescence intensity L with respect to the absorption A for many samples with different surface conditions. These include surfaces ground by grinding papers or finished with various diamond pastes, as well as a high quality film evaporated on an optically flat Si substrate. The dependence is approximated by the function $L \propto A^{2.64}$. The effect of the absorption strength is responsible for both the excitation and emission processes. In Eq. (1), $\varepsilon(E_\mathrm{exc}) = A$ and $\varepsilon(E_\mathrm{L})$ at $E_\mathrm{L} = 0.9$ is approximated as $\varepsilon(E_\mathrm{exc})$, because the energy difference is not large. Since the peak intensity has a $I^{1.3}$ dependence on the incident light intensity at relatively

low excitation intensity, according to Fig. 3(b), the effect of the absorption strength is proportional to $A^{1.3}$. Then we obtain the relationship $L \propto A^{2.3}$, which is close to that obtained experimentally from Fig. 5(a). From this result, we conclude that the significant increase of the luminescence intensity is essentially caused by the increase of emissivity (absorption) accompanying the roughening of the surface. Figure 5(b) shows a typical surface profile of a sandblasted sample measured with a laser confocal microscope. The surface has a submicron fluctuation with a root mean square deviation of 0.14 μm. According to the study of thermal radiation from metals with surface structures [21], the fluctuation with a lateral wavelength close to the relevant light wavelength (1 $\sim$ 4 μm) is expected to play important role in coupling between the electromagnetic waves inside and outside the sample.

D. Comparison with other methods

The information obtained from time-resolved luminescence spectroscopy is similar to what would be obtained from TrPES [11,20]. The femtosecond luminescence measurement is applicable to a wide energy range (0.3 to 1.05 eV in this case) and accessible directly to the electron distribution as TrPES is. However, ultrahigh vacuum conditions or a clean surface are not required in luminescence measurements. This is a practically significant advantage over TrPES.

Pump and probe transient absorption/reflection measurement is another group of methodology widely used in investigation of ultrafast phenomena in bulk [26,27] and nanoscale metals [28,29]. The sensitivity and time resolution are very high and important parameters such as electron temperature, cooling time constant, ballistic transport, and diffusion velocity [25,30] are obtained. Nevertheless, in most of the cases, the information about the electron distribution itself is rather indirect, because the interpretation of the response rely on the model involving frequency integrated dielectric properties.

We propose this ultrafast IR luminescence spectroscopy method as an alternative approach to ultrafast optical observations of metals, for which the usefulness of the luminescence spectroscopy has not been widely recognized. Nevertheless, it should be noted that the model used in this report is very simple, neglecting many important factors such as the energy dependence of the thermalization rate, ballistic and diffusive motion of the carriers, optical transition probability, energy dependence of DOS, and emissivity spectrum. The development of a more precise theory is required to elucidate reliable dynamical parameters and to apply this method to other metals with more complicated band structures near the Fermi level. Understanding the luminescence mechanism of metals is important for identifying the properties of not only bulk metals but also metal nanostructures, which receive considerable attention for application as catalysts [31] in environmental engineering and as imaging markers in biology and medical science [32,33]. Relatively strong luminescence of gold in a very wide range (1200–4100 nm) may be useful for biomedical purpose, because the near-infrared window of the biological tissue (650–1350 nm) is included.

V. CONCLUSIONS

Ultrafast luminescence was observed in the IR region for Au and the major behaviors were interpreted in terms of a simple model, assuming nonthermal and thermal distributions for excited electrons. In addition, the three orders of magnitude enhancement in luminescence intensity by surface roughness is ascribed to the increase of the absorption and emissivity.

ACKNOWLEDGMENTS

The authors acknowledge Prof. Y. Kobayashi and Dr. S. Tani at ISSP, The University of Tokyo, for the Yb-laser technology and their advice in the design of the high-performance upconversion spectrometer system. They also thank Prof. N.Yokoshi and Prof. H. Ishihara for critical reading of the manuscript and valuable discussion. This work has been supported by a Grant-in-Aid for Scientific Research (C) (Grant No. 17K05505) from JSPS.

[1] L. Rota, P. Lugli, T. Elsaesser, and J. Shah, Phys. Rev. B **47**, 4226 (1993).
[2] X. Q. Zhou, H. M. van Driel, and G. Mak, Phys. Rev. B **50**, 5226 (1994).
[3] G. Mak and W. W. Rühle, Phys. Rev. B **52**, R11584 (1995).
[4] T. Suemoto, S. Sakaki, M. Nakajima, Y. Ishida, and S. Shin, Phys. Rev. B **87**, 224302 (2013).
[5] Shun-ya Maezawa, H. Watanabe, M. Takeda, K. Kuroda, T. Someya, I. Matsuda, and T. Suemoto, Sci. Rep. **5**, 16443 (2015).
[6] A. Mooradian, Phys. Rev. Lett. **22**, 185 (1969).
[7] *Surface Enhanced Raman Scattering*, edited by R. K. Chang and T. E. Furtak (Plenum, New York, 1982).
[8] G. T. Boyd, Z. H. Yu, and Y. R. Shen, Phys. Rev. B **33**, 7923 (1986).
[9] M. R. Beversluis, A. Bouhelier, and L. Novotny, Phys. Rev. B **68**, 115433 (2003).
[10] J. Shah, IEEE J. Quantum Electron. **QE-24**, 276 (1988).
[11] W. S. Fann, R. Storz, H. W. K. Tom, and J. Bokor, Phys. Rev. B **46**, 13592 (1992).
[12] A. P. Cracknell, in *Electron States and Fermi Surfaces of Elements*, Landolt-Börnstein - Group III, Condensed Matter (Springer, Cham, 1984), Vol. 13C.
[13] V. E. Gusev and O. B. Wright, Phys. Rev. B **57**, 2878 (1998).
[14] P. B. Allen, Phys. Rev. Lett. **59**, 1460 (1987).
[15] V. V. Kabanov and A. S. Alexandrov, Phys. Rev. B **78**, 174514 (2008).
[16] V. V. Baranov and V. V. Kabanov, Phys. Rev. B **89**, 125102 (2014).
[17] R. H. M. Groeneveld, R. Sprik, and Ad. Lagendijk, Phys. Rev. B **51**, 11433 (1995).
[18] C. Suarez, W. E. Bron, and T. Juhasz, Phys. Rev. Lett. **75**, 4536 (1995).
[19] M. Lisowski, P.A. Loukakos, U. Bovensiepen, J. Stähler, C. Gahl, and M. Wolf, Appl. Phys. A **78**, 165 (2004).
[20] M. Bauer, A. Marienfeld, and M. Aeschlimann, Prog. Surf. Sci. **90**, 319 (2015).
[21] W. Li and S. Fan, Opt. Exp. **26**, 15995 (2018).

[22] H. Sai, H. Yugami, Y. Akiyama, Y. Kanamori, and K. Hane, Opt. Soc. Am. A **18**, 1471 (2001).
[23] H. Sai, Y. Kanamori, and H. Yugami, Appl. Phys. Lett. **82**, 1685 (2003).
[24] P. J. Hesketh, J. N. Zemel, and B. Gebhart, Nature (London) **324**, 549 (1986).
[25] S. Löfving, Appl. Phys. Lett. **36**, 633 (1980).
[26] J. Hohlfeld, S. -S. Wellershoff, J. Güdde, U. Conrad, V. Jähnke, and E. Matthias, Chem. Phys. **251**, 237 (2000).
[27] N. Del Fatti, C. Voisin, M. Achermann, S. Tzortzakis, D. Christofilos, and F. Vallée, Phys. Rev. B **61**, 16956 (2000).
[28] N. Del Fatti, F. Vallée, C. Flytzanis, Y. Hamanaka, and A. Nakamura, Chem. Phys. **251**, 215 (2000).
[29] Sunil Kumar and A. K. Sood, *Ultrafast Response of Plasmonic Nanostructures*, in Reviews in Plasmonics, edited by C. Geddes (Springer, Cham, 2016),Vol. 2015.
[30] X. Liu, R. Stock, and W. Rudolph, Phys. Rev. B **72**, 195431 (2005).
[31] M. Haruta and M. Daté, Appl. Catal. A **222**, 427 (2001).
[32] J. Zheng, C. Zhou, M. Yu, and J. Liu, Nanoscale **4**, 4073 (2012).
[33] M. Hu, J. Chen, Z.-Y. Li, L. Au, G. V. Hartland, X. Li, M. Marquez, and Y. Xia, Chem. Soc. Rev. **35**, 1084 (2006).